Adaptive Control and Filtering for Closed-Loop Adaptive-Optical Wavefront Reconstruction

Troy A. Rhoadarmer and Laura M. Klein

Optics Division, AFRL/DES, Directed Energy Directorate
U.S. Air Force Research Laboratory, Kirtland AFB, NM 87117-5776 USA

Steve Gibson, Neil Chen and Yu-Tai Liu

Mechanical and Aerospace Engineering
University of California, Los Angeles 90095-1597 USA

ABSTRACT

This paper discusses the application of adaptive control methods in the Atmospheric Simulation and Adaptive-optics Laboratory Testbed at the Starfire Optical Range at the Air Force Research Laboratory, Kirtland AFB. Adaptive compensation is useful in adaptive optics applications where the wavefronts vary significantly from one frame to the next or where wind velocities and the strength of atmospheric turbulence change rapidly, rendering classical fixed-gain reconstruction algorithms far from optimal. The experimental results illustrate the capability of the adaptive control scheme to increase Strehl ratios and reduce jitter.

Keywords: Adaptive control, adaptive optics, jitter

1. INTRODUCTION

Adaptive optics (AO) refers to the use of deformable mirrors (DM) driven by active control loops that feedback wavefront sensor (WFS) measurements to compensate for turbulence-induced phase distortion of optical waves propagating through the atmosphere.[1–5] These control loops reconstruct (i.e., estimate and predict) the phase profile, or wavefront, from the WFS data. The control loops in classical AO systems are linear and time-invariant (LTI), having fixed gains based on assumed statistics of atmospheric turbulence. Such control loops are not themselves adaptive in the sense in which the term *adaptive* is used in the control and filtering literature, where *adaptive* normally refers to updating control and/or filter gains in real time.

Adaptive compensation is needed in many AO applications because wind velocities and the strength of atmospheric turbulence can change rapidly, rendering any fixed-gain reconstruction algorithm far from optimal. Recently, adaptive wavefront reconstruction algorithms based on recursive least-squares (RLS) estimation of optimal reconstructor matrices have been proposed.[6–13] In this approach, an adaptive control loop augments a classical AO feedback loop. Results in[7–9] have shown that the type of adaptive loops used here are robust with respect to modeling errors and sensor noise.

The Atmospheric Simulation and Adaptive-optics Laboratory Testbed (ASALT) at the Starfire Optical Range at the Air Force Research Laboratory, Kirtland AFB, has proved to be an ideal laboratory facility for the development and evaluation of advanced AO concepts like the adaptive control and filtering algorithms developed at UCLA. The ASALT Lab provides a well-controlled environment for testing as well as a flexible architecture for integrating new hardware and software components. Several AO systems are available for use in the ASALT Lab. A diagram of the optical system used to test the adaptive reconstruction algorithms is shown in figure 2. The system contains a turbulence simulator, a 577-channel DM, a couple different WFSs, and a number of scoring sensors. The main elements of the ASALT Lab that have particular relevance to this project are described in the next section. The remainder of the paper provides an overview of the adaptive control algorithm used here and presents initial experimental results from the ASALT laboratory.

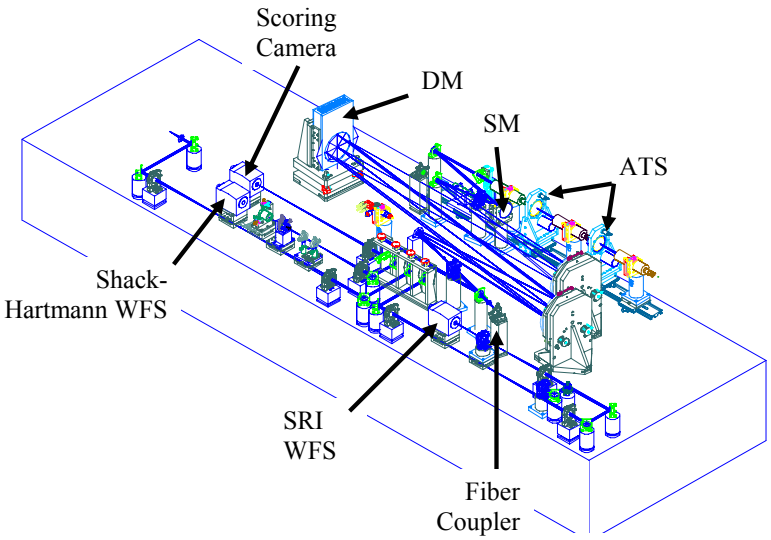

Figure 1. Atmospheric Simulation and Adaptive-optics Laboratory Testbed (ASALT) optical system.

2. THE ADAPTIVE OPTICS LABORATORY AT THE STARFIRE OPTICAL RANGE

2.1. Atmospheric Turbulence Simulator

The Atmospheric Turbulence Simulator (ATS) allows laboratory tests to be performed in the presence of realistic atmospheric turbulence.[14,15] The ATS simulates a two-layer atmosphere using static phase plates imprinted with Kolmogorov statistics and is capable of generating a wide range of atmospheric conditions. One of the phase plates is used to simulate a low-altitude atmospheric layer while the other simulates a high-altitude layer. The two phase plates are located in back-to-back afocal systems. By placing the phase plates in converging portions of the beam, the magnitude of r_0 can be controlled by moving the plates up or down the beam path. Scintillation can be controlled by selecting appropriate field lenses within each afocal system to adjust the effective altitude of the turbulence layers. In addition, stepper motors are used to rotate the phase plates through the optical beam. The motors control the rotational speed of the plates and provide control of the Greenwood frequency. They also control the rotational position of the plates so that turbulence scenarios can be repeated.

2.2. Deformable mirror

After exiting the ATS, the aberrated beam is relayed to a steering mirror (SM) and then to the DM. The SM and DM are both conjugate to the system pupil. The DM is a Xinetics 577-channel continuous surface mirror with 8 μm of physical stroke and a 7.7 mm actuator spacing. The pupil diameter at the DM is set so 25 actuators fit across the pupil. While the DM can operate at several kilohertz, the system frame rate is limited to about 10 Hz due to PC sequential processing as well as the use of commercial IR cameras from Indigo for the WFS and focal plane scoring cameras.

2.3. SRI WFS

The testbed currently contains two WFSs—a Self-Referencing Interferometer (SRI) WFS[16,17] and a Shack-Hartmann WFS. The SRI WFS was used for this project. After reflection from the SM and DM, part of the optical beam is used for the WFS beacon and another portion is coupled into a single mode fiber to form the SRI reference. At the output of the fiber path, a lens collimates the reference so it can be recombined with the beacon beam on the SRI WFS camera. The SRI WFS currently implements temporal phase shifting using an inline fiber phase shifter. However, since data flow and processing are controlled and synchronized by the computer

E-mail: gibson@ucla.edu, yutai@ucla.edu

system as described below, spatial phase shifting was simulated by capturing all four of the interference images during the same time step of the AO system control loop. The camera used for the SRI WFS, as well as the scoring camera, is a mid-format Indigo Phoenix camera.

2.4. Computer control system

The ASALT control system provides a well-defined, modular architecture for integrating and linking hardware and software elements. The basic building block of the system is a component, which is similar to an object in object-oriented programming. Components can be elements such as frames sources (i.e., sensors and detectors), DM or tracking controllers, atmospheric simulators, and processing nodes. Each component has defined input and output interfaces which allow it to accept data from and send data to other components. Multiple components can be linked together to perform a desired function, such as closing an AO control loop. The modular architecture provides a large amount of flexibility for constructing experiments. The underlying application programming interface (API) controls the flow and synchronization of data between components, ensuring that only compatible inputs and outputs are connected and that a component is initiated only when all of its inputs are satisfied. It also provides for the recording of any data which flows through the system for later performance analysis.

All of the components for the testbed run on personal computers, although it is possible to incorporate other platforms. A shared memory backbone is used to pass information between computers. Writing and reading of data from the shared memory is handled by the API through a set of library functions created for use within each component's software interface. Currently, C/C++ and Matlab interfaces are available for the library. The Matlab interface has proven to be particularly useful for this project. Computer simulations of the adaptive control and filtering algorithms were previously implemented and tested in Matlab. With this interface, the simulation routines were quickly converted to functional components for the ASALT laboratory.

3. ADAPTIVE OPTICS AND ADAPTIVE CONTROL

The adaptive optics problem is represented by the block diagram in Figure 2. The measured wavefront vector is denoted by y, and the command vector to the deformable mirror (DM) is denoted by c. The objective of the control loops is to minimize the RMS value, over space and time, of the projection of y onto a certain subspace.

The top two feedback loops in Figure 2 are classical AO and track loops, with integrator gains K_1 and K_2, respectively. These feedback loops are linear time-invariant (LTI) control loops. The blocks in Figure 2 labeled z^{-d} represent total loop latency, usually due to computation and sensor read-out delays. In the experiment reported here, the loop latency is $d = 1$.

The matrix V in the AO loop defines a parameterization of actuator space. The columns of V represent orthogonal DM modes that are commanded independently by the control loop. Thus,

$$c = Vv \tag{1}$$

where the vector v contains the independent control commands generated by the AO loops, and the vector c contains the individual master actuator commands. Similar parameterizations have been used previously,[8–10] but the method for computing frequency weighted DM modes in Section 5 of this paper produces more desirable DM modes. As discussed in Section 5, tilt was removed from the modes used for this paper, so that the AO and track loops are uncoupled.

The reconstructor matrix E_0 in the classical AO loop is chosen to satisfy

$$E_0 V = I. \tag{2}$$

Under this hypothesis, the control channels represented by the components of the vector v are uncoupled; i.e., the control command represented by a single element of v affects only the error signal represented by the corresponding element of the error vector

$$\varepsilon = E_0\, y, \tag{3}$$

which is the input to the integrator in the classical AO loop; the signal y is the output of the wavefront sensor.

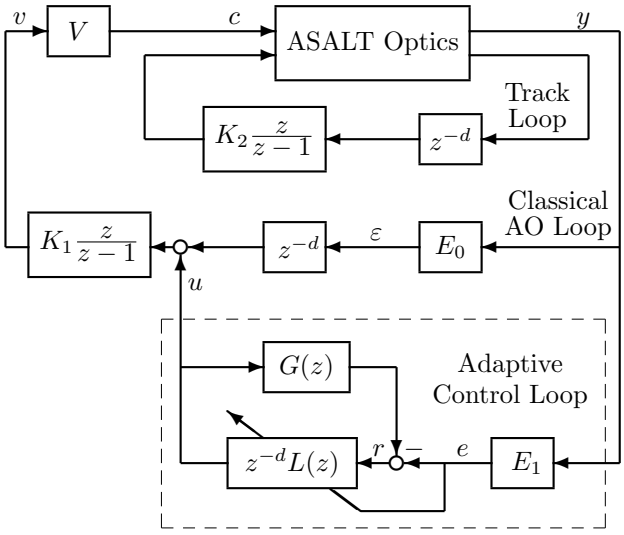

Figure 2. Block diagram of the digital control loops for adaptive optics. ASALT optics block represents the optical system in Figure 1.

In this paper, E_0 is equal to the pseudo inverse of V. Thus, the objective of the classical AO loop is to cancel the orthogonal projection of the wavefront vector y onto the range of V, which is the subspace spanned by the DM modes used by the control loops.

The adaptive control loop is enclosed in the dashed box in Figure 2. This control loop augments the classical AO loop to enhance wavefront prediction and correction, particularly for higher-order wavefront modes. The main component of this loop is the filter $L(z)$. The gains in this filter are updated adaptively. This adaptation may be either fully adaptive (i.e., filter gains are updated at each time step) or quasi adaptive (i.e., filter gains are updated periodically).

For identification of the filter gains, the problem is formulated as a feedforward disturbance-rejection problem with reference signal

$$r = G(z)u - E_1\, y \tag{4}$$

and tuning signal

$$e = E_1 y\,, \tag{5}$$

as indicated in Figure 2. The transfer function $G(z)$ is an approximation to the transfer function from the control signal u to the tuning signal e with only the classical AO loop closed, and E_1 is a constant matrix. Thus, the input to the filter $L(z)$ is r, and the gains in $L(z)$ are identified to minimize the RMS value over time and space of e (equivalently, the RMS value over time of $||e||$).

In this paper, $E_1 = E_0$. The matrix E_1 will be different from E_0 if, for example, the adaptive loop is used for only some of the DM modes controlled by the classical AO loop. In this case, E_1 contains the rows of E_0 corresponding to the DM modes for which the adaptive loop is used.

With the condition (2) and the condition $E_1 = E_0$, the control channels represented by the columns of the matrix V are uncoupled in the classical AO loop. The transfer function $G(z)$ then reduces to the following scalar transfer function for each channel:

$$G(z) = \frac{-K_1\, z^d}{z^d - z^{d-1} + K_1}\,. \tag{6}$$

The filter $L(z)$ in the adaptive control loop could be either FIR or IIR. While an IIR filter theoretically would produce optimal steady-state performance for stationary disturbance statistics, an FIR filter of sufficient order can approximate the steady-state performance of an IIR filter, and the convergence of the adaptive algorithm for an FIR filter is more robust with respect to modeling errors. In most AO problems to which the current

methods have been applied, FIR filter orders greater than eight do not offer further performance improvement. Hence, an FIR filter is used in this paper. As the gains in the filter $L(z)$ are updated repeatedly, they converge to optimal constant gains when the disturbances have constant statistics.

The common form for an FIR filter of order n with input signal r and output signal u is

$$u = \sum_{k=1}^{n} A_k z^{1-k} r \tag{7}$$

where each A_k is a coefficient matrix with dimensions determined by the number of output channels and input channels. The fully adaptive version of the controller here uses a lattice realization of the FIR filter $L(z)$, which is quite different from the realization in (7). The lattice realization is more complex than the realization in (7), but it has important advantages in terms of numerical stability and efficiency in RLS estimation of optimal filter gains for large orders and large numbers of channels. The FIR lattice filter used here is based on the multichannel lattice filter presented in [18], which derives numerical stability and efficiency from an orthogonalization of the data channels.

An important result follows from the fact that, under the condition (2), the control channels are uncoupled in the classical AO loop: The RLS problem for identifying the optimal filter $L(z)$ reduces to a set of independent RLS problems for the gains in the individual rows of $L(z)$. This makes the RLS problem at least tractable for real-time computation, although still challenging because of the large number of channels. The adaptive filtering problem to determine the optimal gains for $L(z)$ is still multichannel, so that the on-line algorithm for adaptively determining the filter gains must be numerically stable in the presence of many channels.

Even though the channels in the signals v, u, and e are uncoupled for the classical AO loop, all channels in the reference signal r feed into each channel of the adaptive control command u. Hence, the channels are coupled with the adaptive loop closed. Specifically, in predicting each channel of the error signal e, the adaptive filter uses the data from all channels, so that the prediction is based on both spatial and temporal information.

4. QUASI-ADAPTIVE CONTROL: FIXED-GAIN FIR LOOP

When the statistics of the turbulence, platform jitter, and any other disturbances are stationary, the gains in the adaptive filter $L(z)$ in the adaptive control loop converge to constant values. Once these steady-state gains have been reached, the adaptive control loop is equivalent to a much simpler controller, in which the filter $L(z)$ is a fixed-gain FIR filter. This suggests an alternative, quasi-adaptive implementation of the FIR augmentation to the classical AO loop for applications where the statistics of the turbulence and other disturbances vary slowly or not at all during an engagement. In the quasi-adaptive implementation, the FIR gains can be estimated from a limited amount of wavefront-sensor data and then applied in the control loop. If necessary, the FIR gains can be updated periodically.

Whether the FIR gains are identified only once or updated periodically, the quasi-adaptive implementation eliminates the significant real-time computational burden of updating the FIR gains in each sampling interval. Because of the large number of sensor channels in the AO problem, the RLS lattice filter used in fully adaptive implementation is used also in the quasi-adaptive implementation to identify the FIR gains, but in the experiments reported here, the FIR realization in (7) was used in the control loop.

For estimation of fixed FIR gains, the classical AO loop and track loop are closed and a sequence of WFS frames is collected and used for least-squares estimation of the FIR gains. For the results in Section 6, the RLS lattice filter was used to identify the gains, but in principle, a batch least-squares method could be used.

There also are options for how the wavefront data used in the identification is collected. The most obvious option, which was used for the results reported here, is to collect a single sequence of consecutive wavefront frames. For the experiment described in this paper, 3000 consecutive frames were used to identify the FIR gains.

In the second method used for collecting wavefront data for identification of the FIR gains, smaller numbers (typically 1000) of consecutive frames can be saved from each of several different experiments with independent but statistically equivalent turbulence, and these sequences can be conjoined to produce a single longer data

sequence. Since the basic idea in identifying the FIR gains is to identify correlations between the wavefront sequence and backward shifts of itself, the number of independent sequences that can be conjoined is limited because the correlations will not hold across the boundary between two sequences. This method has proved successful in simulations of AO problems.[12, 13]

A final important point about identification of the FIR gains must be made. The performance of the fixed-gain FIR loop must be evaluated on a different turbulence sequence from that used to identify the gains, although the two turbulence sequences should have the same statistics.

5. FREQUENCY-WEIGHTED DEFORMABLE MIRROR MODES

Orthogonal DM modes are essential for the adaptive control scheme discussed in Sections 3 and 4 for two reasons: (1) so that $||e||$ is a physically meaningful least-squares objective function for identification of the adaptive filter gains; (2) well chosen modes permit the use of significantly fewer control channels, thus greatly reducing the real-time computational burden of the adaptive control loop.

Several methods for developing orthogonal deformable-mirror modes for use in adaptive optics with adaptive control have been introduced in [8–10]. These methods yielded useful modes, but they had certain undesirable features. The methods in [8, 9] require a gramian matrix for the actuator influence functions that usually is not available for real deformable mirrors, and the method in [10] tends to produce modes with mixed low and high spatial frequency content.

The frequency-weighted DM modes used in this paper eliminate mixing of low and high spatial frequencies. The method used here is described in detail in a recent paper.[13] This method produces a sequence of orthogonal DM modes that are ordered according to spatial frequency content so that the first modes in the sequence are very smooth and the dominant spatial frequencies increase with the mode number. Figure 3 shows representative modes from the 447 orthogonal tilt-removed DM modes computed for the experiment discussed in this paper. Only the first 150 modes were used for the experimental results reported here.

The method for computing the DM modes used here requires only the actuator geometry.[13] No information about the statistics of atmospheric turbulence is used. If there is any pre-imposed actuator slaving, the a matrix defining this slaving is required. If, as is common in AO applications, tilt-removed DM modes are desired, a set of tilt-removed basis vectors in actuator space is required. These initial vectors usually are computed using a poke matrix for the DM-WFS combination; they need not be orthogonal or frequency-weighted in any sense.

Low-pass spatial filtering has been used previously in classical AO loops to eliminate high-frequency noise from DM commands. Notably, low-pass filtering the reconstructed phase was shown in [19] to mitigate the effect of misregistration of actuator and sensor geometry. The way that the frequency-weighted DM modes are used here has the effect of first low-pass filtering the WFS vector and then generating DM commands with limited spatial-frequency bandwidth. The idea of frequency-weighted DM modes is new, although a relevant precedent is [9], where Zernike functions were approximated by linear combinations of actuator influence functions and the resulting DM shapes orthogonalized. Of course, generating DM modes by approximating Zernikes is not new, but for finite numbers of actuators and most aperture geometries the resulting DM modes are not orthogonal as needed for adaptive control. The process of building the discrete approximations to Zernikes and then re-orthogonalizing as in [9] is tedious for complicated DM geometries, particularly with slaved actuators, and does not appear to be guaranteed to preserve separation of low and high spatial frequencies.

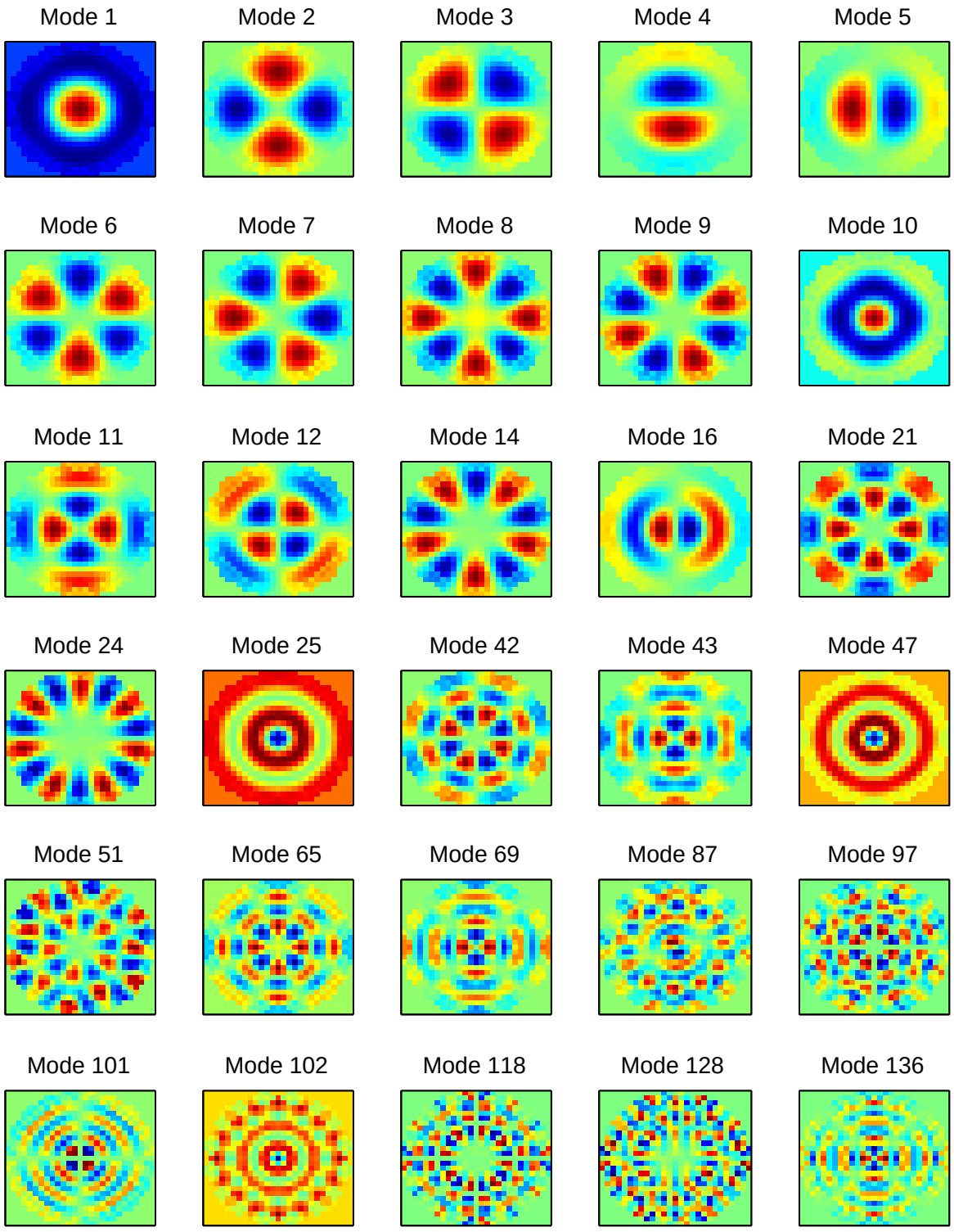

Figure 3. Representative frequency-weighted deformable mirror modes used for this paper.

6. EXPERIMENTAL RESULTS

Tests were performed in the ASALT laboratory to evaluate the performance of the quasi-adaptive version of the adaptive control loop. In these tests, the first 150 DM modes were used by the adaptive control loop. For comparison, tests on the same turbulence were performed also with only the classical AO an track loops, using 150 modes in one case and commanding all 447 master actuators independently in another case. Commanding all master actuator independently is equivalent to using all of the DM modes, so that this case is referred to as "all modes" in the results presented here.

Figure 4 shows the time history of the Strehl ratios for the three closed-loop tests, and Table 1 lists the average Strehls and standard deviations. The Strehls were calculated from the scoring camera images. Figure 5 shows typical images for a single frame. Previous experiments with weaker turbulence than that used for the results here had indicated that using more than 150 DM modes did not yield higher Strehls; however, Figure 4 and Table 1 show that using more than 150 modes in the experiments reported here does increase the Strehls, but at the expense of more variation, as shown by the time series in Figure 4 and the higher standard deviation in Table 1. The quasi-adaptive (i.e., fixed-gain FIR loop) with only 150 modes produces higher Strehls than the classical AO loop with all modes, and with reduced variation. This is possible because the FIR filter combines spatial and temporal prediction of the wavefront to minimize the wavefront error. It appears likely that the adaptive control loop would perform even better if more modes were used.

Figures 6 and 7 show the jitter of the centroids of the images. As with the Strehls, the jitter is improved by using all DM degrees of freedom (all modes) as opposed to only the first 150 modes, but the quasi-adaptive controller using only 150 modes significantly reduces the jitter as compared to classical AO with all modes. It should be noted that the quasi-adaptive loop works on only the tilt-removed part of the wavefront, so that the jitter reduction achieved by the quasi-adaptive loop is due entirely to improved higher-order wavefront correction. It is expected that adaptive control of tilt jitter as in [12, 20, 21] would reduce the centroid jitter even more.

Table 1. Average Strehl Ratios for 1000 Frames

AO Loop	Average Strehl	Standard Deviation
Classical AO 150 modes	0.2769	0.0975
Classical AO and FIR loop 150 modes	0.4057	0.0811
Classical AO all modes	0.3432	0.1180

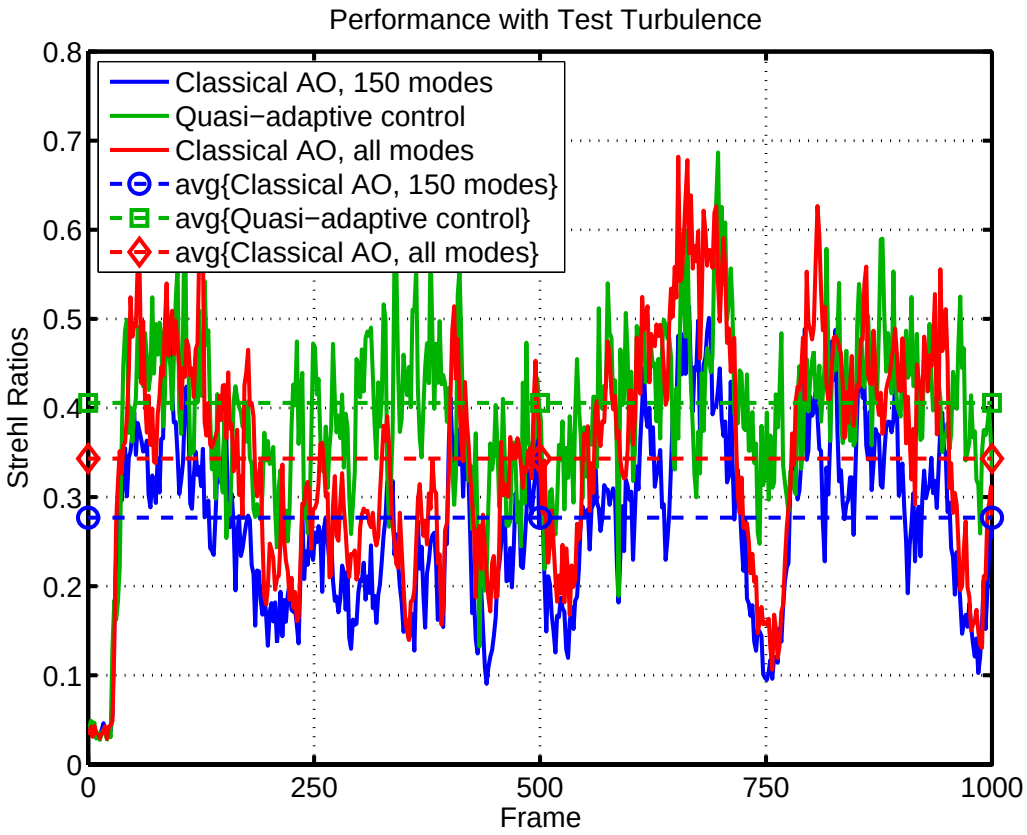

Figure 4. Experimental Strehl ratios. As shown on the graph, the AO loop was initially closed at frame 30.

7. CONCLUSIONS

A quasi-adaptive controller for adaptive optics, developed at UCLA, has been implemented in hardware at the ASALT laboratory at the Starfire Optical Range, Air Force Research Laboratory, Kirtland AFB. This controller can be used to augment classical AO and track loops. The quasi-adaptive loop improves wavefront correction because the FIR filter in this loop performs temporal prediction, which classical AO loops cannot do. The experimental results here demonstrate that the quasi-adaptive loop achieves higher Sthrel ratios on the scoring camera, as well as lower variation of the Strehls, than the classical AO loop alone achieves.

The results produced by a classical AO loop alone using all deformable mirror modes and using the 150 modes used for the quasi-adaptive loop suggest that the quasi-adaptive loop should produce even higher performance with more modes, so future experiments will investigate this. Also, future experiments are planned to implement the fully adaptive version of the UCLA controller, as well as compare performance between the SRI and Shack-Hartmann wavefront sensors in the ASALT laboratory.

ACKNOWLEDGMENTS

This work was supported by the U. S. Air Force Office of Scientific Research under AFOSR Grants F49620-02-01-0319 and F-49620-03-1-0234 and AFOSR Laboratory Task LRIR-93DE01COR.

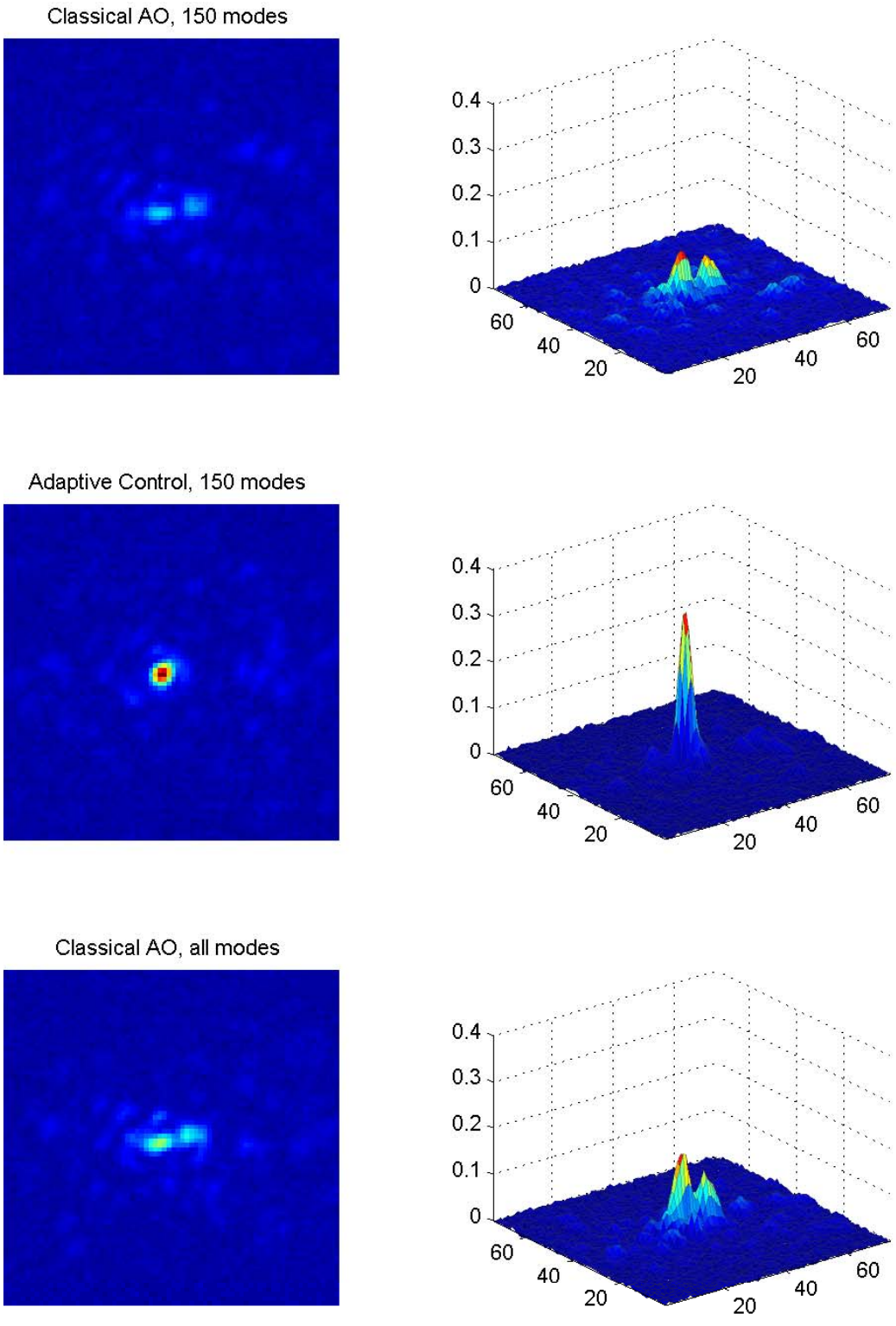

Figure 5. Representative closed-loop scoring camera images.

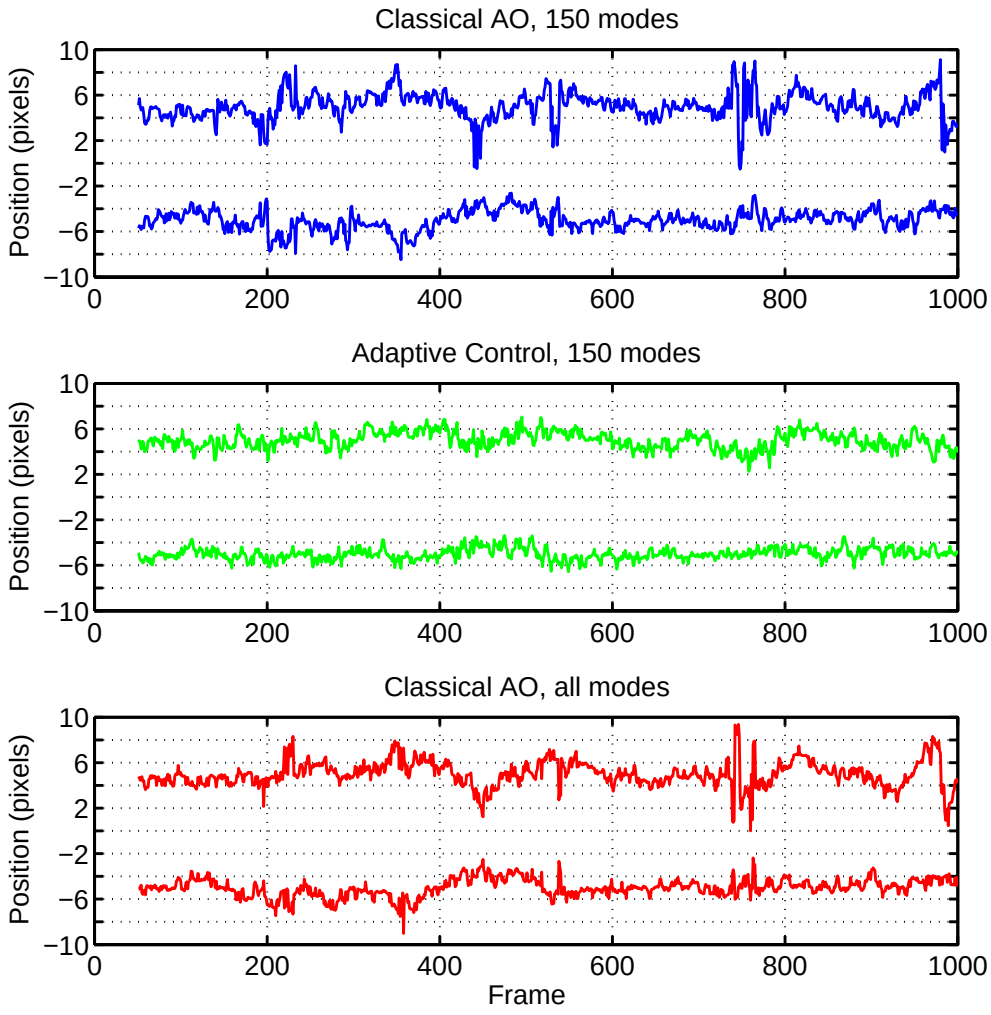

Figure 6. Closed-loop centroid jitter in units of pixels on the scoring camera. The top curve in each graph represents the x-axis jitter and the bottom curve represents the y-axis jitter.
Top: classical AO with 150 DM modes; standard deviation $(x, y) = (1.2335, 0.8791)$.
Middle: adaptive control with 150 DM modes; standard deviation $(x, y) = (0.7522, 0.5139)$.
Bottom: classical AO with all DM modes; standard deviation $(x, y) = (1.1553, 0.7905)$.

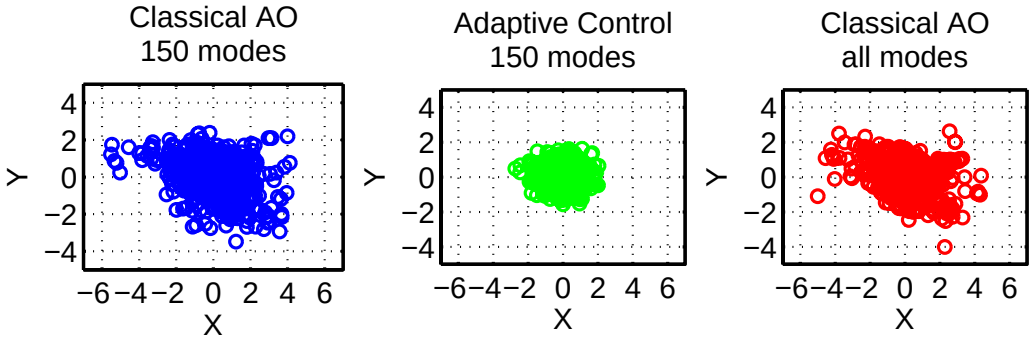

Figure 7. Closed-loop centroid scatter relative to mean spot position, in units of pixels on the scoring camera.

REFERENCES

1. J. W. Hardy, "Adaptive optics," *Scientific American* **270**(6), pp. 60–65, 1994.
2. G. Rousset and J. C. Fontanella et al., "First diffraction limited astronomical images with adaptive optics," *Astron. and Astrophys.* **230**, pp. L29–L32, 1990.
3. R. Q. Fugate and B. L. Ellerbroek et al., "Two generations of laser guide star adaptive optics experiments at the starfire optical range," *J. Opt. Soc. Am. A* **11**, pp. 310–324, 1994.
4. B. L. Ellerbroek, C. Van Loan, N. P. Pitsianis, and R. J. Plemmons, "Optimizing closed-loop adaptive optics performance using multiple control bandwidths," *J. Opt. Soc. Am. A* **11**, pp. 2871–2886, 1994.
5. M. Lloyd-Hart and P. McGuire, "Spatio-temporal prediction for adaptive optics wavefront reconstructors," in *Adaptive Optics*, M. Cullum, ed., **ESO Conf. Proc. 54**, pp. 95–101, (European Sourthern Observatory, Garching), 1996.
6. B. L. Ellerbroek and T. A. Rhoadarmer, "Real-time adaptive optimization of wave-front reconstruction algorithms for closed-loop adaptive-optical systems," in *Adaptive Optical System Technologies*, D. Bonaccini and R. Tyson, eds., *SPIE Proc.* **3353**, pp. 1174–1183, 1998.
7. J. S. Gibson, C.-C. Chang, and B. L. Ellerbroek, "Adaptive optics: Wavefront reconstruction by adaptive filtering and control," in *38th IEEE Conference on Decision and Control*, IEEE, (Phoenix, Arizona), December 1999.
8. J. S. Gibson, C.-C. Chang, and B. L. Ellerbroek, "Adaptive optics: wavefront correction by use of adaptive filtering and control," *Applied Optics, Optical Technology and Biomedical Optics* , pp. 2525–2538, June 2000.
9. C.-C. Chang and J. S. Gibson, "Parallel control loops based on spatial subband processing for adaptive optics," in *American Control Conference*, IEEE, (Chicago), June 2000.
10. J. S. Gibson, C.-C. Chang, and Neil Chen, "Adaptive optics with a new modal decomposition of actuator and sensor spaces," in *American Control Conference*, (Arlington, VA), June 2001.
11. Y.-T. Liu and J. S. Gibson, "Adaptive optics with adaptive filtering and control," in *American Control Conference*, (Boston, MA), June 2004.
12. Yu-Tai Liu, Neil Chen, and Steve Gibson, "Adaptive filtering and control for wavefront reconstruction and jitter control in adaptive optics," in *American Control Conference*, (Portland, OR), June 2005.
13. Yu-Tai Liu and Steve Gibson, "Adaptive control in adaptive optics for directed energy systems," sumbitted to *Optical Engineering* .
14. S. V. Mantravadi and T. A. Rhoadarmer, "Simple laboratory system for generating well-controlled atmospheric-like turbulence," *Proc. SPIE* , pp. 290–300.
15. S. M. Ebstein, "Pseudo-random phase plates," *Proc. SPIE* , pp. 150–155.
16. T. A. Rhoadarmer, "Development of a self-referencing interferometer wavefront sensor," *Proc. SPIE* , pp. 112–126.
17. J. D. Barchers, D. L. Fried, D. J. Link, G. A. Tyler, W. Moretti, T. J. Brennan, and R. Q. Fugate, "Performance of wavefront sensors in strong scintillation," *Proc. SPIE* , pp. 217–227.
18. S.-B. Jiang and J. S. Gibson, "An unwindowed multichannel lattice filter with orthogonal channels," *IEEE Transactions on Signal Processing* **43**, pp. 2831–2842, December 1995.
19. Terry J. Brennan, "Stability margin loss due to wavefront sensor misregistration: amelioration with spatial filtering techniques," in *Proceedings of SPIE*, **4376**, pp. 88–98, 2001.
20. Néstor O. Pérez Arancibia, Neil Chen, Steve Gibson, and Tsu-Chin Tsao, "Variable-order adaptive control of a MEMS steering mirror for suppression of laser beam jitter," to appear in *Optical Engineering* .
21. Néstor O. Pérez Arancibia, Neil Chen, Steve Gibson, and Tsu-Chin Tsao, "Adaptive control of a MEMS steering mirror for suppression of laser beam jitter," in *American Control Conference*, IEEE, (Portland, OR), June 2005.